

Journal of Materials Chemistry C

Accepted Manuscript



This is an *Accepted Manuscript*, which has been through the Royal Society of Chemistry peer review process and has been accepted for publication.

Accepted Manuscripts are published online shortly after acceptance, before technical editing, formatting and proof reading. Using this free service, authors can make their results available to the community, in citable form, before we publish the edited article. We will replace this *Accepted Manuscript* with the edited and formatted *Advance Article* as soon as it is available.

You can find more information about *Accepted Manuscripts* in the [Information for Authors](#).

Please note that technical editing may introduce minor changes to the text and/or graphics, which may alter content. The journal's standard [Terms & Conditions](#) and the [Ethical guidelines](#) still apply. In no event shall the Royal Society of Chemistry be held responsible for any errors or omissions in this *Accepted Manuscript* or any consequences arising from the use of any information it contains.

Cite this: DOI: 10.1039/c0xx00000x

PAPER

www.rsc.org/xxxxxx

Synergetic effect of C*N[^]N/C[^]N[^]N coordination and the arylacetylide ligands on the photophysical properties of cyclometalated platinum complexes

Wenting Wu^{a,b} Xueyan Wu,^a Jianzhang Zhao^{b,*} and Mingbo Wu^{a,*}

Received (in XXX, XXX) Xth XXXXXXXXX 20XX, Accepted Xth XXXXXXXXX 20XX

DOI: 10.1039/b000000x

Six coordinated Pt(II) complexes were prepared, in which the C*N[^]N or the C[^]N[^]N ligand were used to form Pt(II) coordination center. For each coordination profile, three different arylacetylide ligands were used, i.e. naphthalenedimide (NDI), pyrenyl (Py) and naphthaleneimide (NI) acetylides. The electrochemical and the photophysical properties of the complexes were studied with steady-state and time-resolved absorption and emission spectroscopies, cyclic voltammetry and DFT calculations. The photostability and the photoluminescent properties of the complexes are finely tuned by the photoredox and photochemical properties of the arylacetylide ligands and C*N[^]N/C[^]N[^]N Pt(II) coordination center. The triplet excited states of the complexes are in intraligand feature and the lifetime is long (90.1 μs). The photophysical properties of the complexes were rationalized with DFT calculations. The complexes were used as triplet photosensitizer for triplet-triplet annihilation upconversion, the upconversion quantum yield is up to 29.7 %. The results are useful for future designing of the Pt(II) complexes showing strong visible light-absorption, RT phosphorescence and long-lived triplet excited states.

Introduction

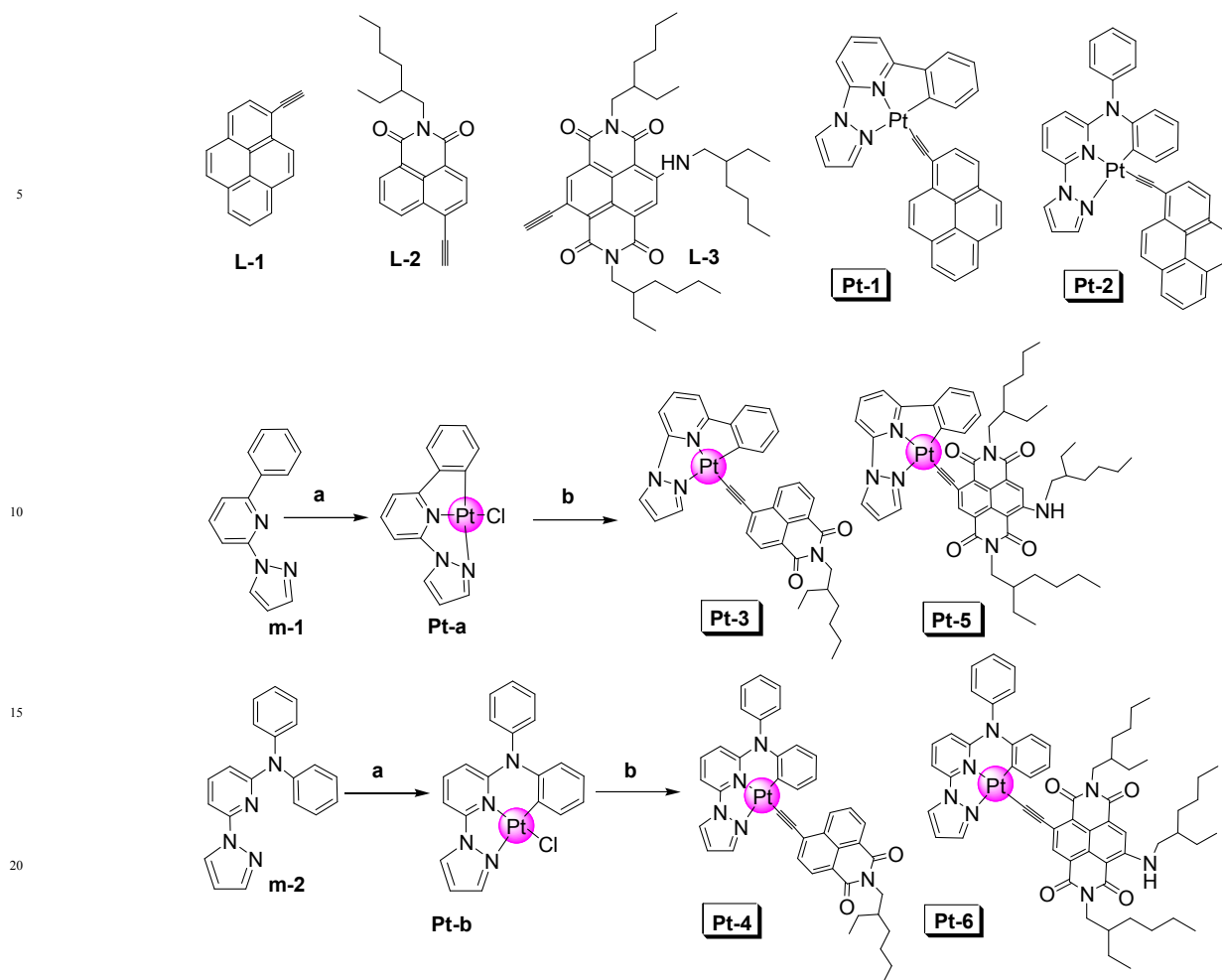
Platinum (II) complexes have attracted much attention due to their fascinating photophysical properties, such as tunable absorption/emission wavelength, and feasibly derivatizable molecular structures. These complexes have been widely used in electroluminescence photoorganic reactions,¹ photocatalytic hydrogen (H₂) production,² phosphorescent molecular probes,^{3–5} singlet oxygen sensitization⁶ and triplet-triplet annihilation upconversion.^{7–9}

Recently, a great deal of efforts have been devoted to develop C[^]N or C[^]N[^]N ligands to obtain a planar geometry for the Pt(II) coordination center, with which the photoluminescence can be enhanced.^{11–13} Different arylacetylide ligands were also used to enhance the visible-light-harvesting ability and prolong the lifetime of triplet excited state.^{8,9,14–19} Our group prepared N[^]N Pt(II) complexes with acetylide ligands based on Bodipy,²⁰ naphthalimide (NI),²¹ naphthalenediimide (NDI),²² pyrene (Py),²¹ rhodamine,²³ fluorescein²⁴ and coumarin moieties.²⁵

However, most studies of these Pt(II) complexes are focused on the optimization of π-conjugation or simply introducing arylacetylide ligands. Actually, geometry for the Pt(II) coordination center, charge transfer process (MLCT) and energy transfer process (Intraligand energy transfer, IL←MLCT) have

great synergic effects on the photophysical properties of Pt(II) complexes. Pt(II) coordination center as triplet spin convertor plays an important role in the triplet photosensitizers, due to efficient intersystem crossing (¹MLCT→³MLCT). Furthermore, charge transfer process and energy transfer process may compete with each other. It is highly desired to develop molecular structure designing rationales for Pt(II) complexes to tune the driving forces for charge transfer and energy transfer, when the geometry for the Pt(II) coordination center is in the stationary state.

Organic fluorophore can absorb visible light, and their photoredox properties (driving forces for charge transfer) and their energy levels of emission and absorption can be finely modified by rational design and synthesis.²⁶ Herein we studied the aforementioned synergetic effect based on the C[^]N[^]N/C*N[^]N coordination protocol developed by Huo et al.²⁷ Six Pt(II) complexes with two different coordination ligands, i.e. the C*N[^]N with five–six fused metallacycle, or the C[^]N[^]N with five–five fused metallacycle, were prepared. On the other hand, with different singlet/triplet state energy levels and redox properties, three different arylacetylide ligands based on Py, NI and NDI moieties, were used for the construction of the Pt(II) complexes. The photoredox properties of the ligands and complexes were studied with cyclic voltammetry, while the photophysical properties of the complexes were studied with steady-state absorption, time-resolved absorption and



25 **Scheme 1.** Synthesis of the Pt(II) complexes and the structure of the ligands. (a) K_2PtCl_4 (1 equiv.), acetic acid, reflux; 22h; (b) L-2 or L-3, CuI, CH_2Cl_2 , $i-Pr_2NH$, r.t., 24 h.

emission spectroscopy. By introducing electron-withdrawing ligands (L-2 and L-3), the photostability of Pt(II) complexes were enhanced. At the same time, the redox properties and energy level of Pt(II) complexes are finely tuned and the C*N[^]N coordination Pt(II) complexes (Pt-4) show higher phosphorescence quantum yield than that of C[^]N[^]N coordination Pt(II) complexes (Pt-3), which is different from the results of Huo's work.²⁷ The redox and photophysical properties of the complexes were rationalized with DFT calculations. The Pt(II) complexes were used as triplet photosensitizers for triplet-triplet annihilation upconversion.

Experimental Section

Analytical Measurements.

40 All the chemicals used in the syntheses were analytically pure and were used as received. Solvents were dried and distilled. 1-bromopyrene (1), 2-ethylhexyl-4-bromo-1,8-naphthalimide (2), 1,6-dibromonaphthalene-1,2,6,7-tetracarboxylic dianhydrides (3), *N,N'*-di(2-ethylhexyl)-1,6-dibromonaphthalenetetra-4,5-dicarboxylic diimides (4), 4-bromo-2,7-bis(2-ethylhexyl)-9-[(2-ethylhexyl)amino] (5), 2-bromo-6-(1-pyrazolyl)pyridine (6), 2-

phenyl-6-(1H-pyrazol-1-yl)-Pyridine (m-1), *N,N*-diphenyl-6-(1H-pyrazol-1-yl)-2-Pyridinamine (m-2), Pt-a and Pt-b were synthesized according to literature methods (see ESI † for synthesis and the molecular structural characterization data).

55 **Complex Pt-3.** To a 25 mL dry, argon-flushed flask were charged complex Pt-a (45.0 mg, 0.10 mmol), L-2 (43.6 mg, 0.13 mmol), CuI (3.5 mg, 0.018 mmol), *i-Pr*₂NH (1 mL), and dichloromethane (10 mL). The mixture was stirred under Ar at room temperature for 24 h. The crude material was purified by flash chromatography (silica gel, dichloromethane) to give a yellow solid, 35.1 mg, yield 47.0%. M.p.: 208.7–210.3 °C. ¹H NMR (400 MHz, CD₂Cl₂) δ = 9.00 (d, *J* = 8.0 Hz, 1H), 8.57 (d, *J* = 3.5 Hz, 1H), 8.49 (d, *J* = 7.5 Hz, 1H), 8.12 (d, *J* = 3.0 Hz, 1H), 7.92 (d, *J* = 1.5 Hz, 1H), 7.86–7.80 (m, 3H), 7.78–7.75 (t, *J* = 15.5 Hz, 1H), 7.38 (t, *J* = 18 Hz, 2H), 7.21–7.16 (m, 2H), 7.10 (t, *J* = 14 Hz, 1H), 6.68 (t, *J* = 4.5 Hz, 1H), 4.14–4.05 (m, 2H), 1.97–1.92 (m, *J* = 6.8 Hz, 1H), 1.41–1.29 (m, 8H) 0.95–0.88 (m, 6H). ¹³C NMR (100 MHz, CD₂Cl₂) δ = 165.11, 164.85, 164.09, 148.25, 146.59, 144.68, 141.15, 140.21, 137.99, 134.25, 134.06, 133.02, 131.59, 131.30, 131.27, 130.55, 129.98, 128.91, 126.66, 125.34, 124.17, 123.37, 119.15, 115.89, 110.50, 106.64, 103.02, 44.23, 38.35, 31.16, 30.10,

29.16, 24.44, 23.52, 10.87. MALDI-HRMS: calcd ($[\text{C}_{36}\text{H}_{33}\text{N}_4\text{O}_2\text{Pt}+\text{H}]^+$): $m/z = 748.2251$, found $m/z = 748.2239$.

Complex Pt-4. This compound was prepared following the general procedure for complex Pt-3. The crude material was purified by flash chromatography (silica gel, dichloromethane) to give an orange solid, 24.5 mg, yield 46.8%. M.p. >250 °C. ^1H NMR (400 MHz, CD_2Cl_2) $\delta = 9.20$ (d, $J = 24.3, 7.3$ Hz, 1H), 8.62–8.52 (m, 3H), 8.41 (d, $J = 2.7$ Hz, 1H), 8.35 (d, $J = 2.0$ Hz, 1H), 7.98–7.89 (m, 1H), 7.82 (d, $J = 7.4$ Hz, 1H), 7.74–7.57 (m, 6H), 7.22 (t, $J = 8.5$ Hz, 1H), 6.90 (t, $J = 2.0$ Hz, 1H), 6.83 (d, $J = 10.9$ Hz, 1H), 6.74–6.68 (m, 1H), 6.62–6.50 (m, 2H), 4.16–4.05 (m, 2H), 2.01–1.87 (m, 1H), 1.44–0.85 (m, 14H). ^{13}C NMR (100 MHz, CD_2Cl_2) $\delta = 167.98, 165.18, 164.90, 148.82, 147.97, 144.81, 144.11, 142.20, 140.59, 137.07, 134.35, 134.12, 133.21, 132.95, 131.88, 131.31, 131.27, 130.79, 130.02, 129.49, 129.15, 128.99, 128.73, 126.79, 124.47, 123.43, 122.42, 119.37, 119.31, 119.14, 115.42, 114.78, 110.77, 100.40, 98.58, 44.27, 38.41, 31.23, 30.81, 29.20, 24.52, 23.52, 10.9$. MALDI-HRMS: calcd ($[\text{C}_{42}\text{H}_{38}\text{N}_5\text{O}_2\text{Pt}]^+$): $m/z = 839.2637$, found $m/z = 839.2642$.

Complex Pt-5. This compound was prepared following the general procedure for complex Pt-3. The crude material was purified by flash chromatography (silica gel, dichloromethane) to give a red solid, 15.9 mg, yield 32.5%. M.p.: 189.5–191.7 °C. ^1H NMR (400 MHz, CDCl_3) $\delta = 10.02$ (t, $J = 4.4$ Hz, 1H), 8.93–8.82 (m, 2H), 8.42–8.21 (m, 3H), 8.12 (t, $J = 8.1$ Hz, 1H), 7.86 (d, $J = 8.0$ Hz, 1H), 7.71 (d, $J = 7.3$ Hz, 1H), 7.58 (d, $J = 7.0$ Hz, 1H), 7.49 (t, $J = 7.2$ Hz, 1H), 7.12 (t, $J = 7.6$ Hz, 1H), 6.87 (t, $J = 6.8$ Hz, 1H), 4.34–4.03 (m, 4H), 3.51 (t, $J = 5.6$ Hz, 2H), 2.00 (d, $J = 10.3$ Hz, 2H), 1.81 (t, $J = 12.0$ Hz, 1H), 1.56–1.25 (m, 28H), 1.02–0.88 (m, 14H). MALDI-HRMS: calcd ($[\text{C}_{54}\text{H}_{65}\text{N}_5\text{O}_4\text{Pt}+\text{H}]^+$): $m/z = 1056.4751$, found $m/z = 1056.4736$.

Complex Pt-6. The compound was prepared following the general procedure for complex Pt-3. The crude material was purified by column chromatography (silica gel, dichloromethane) to give a red solid, 13.5 mg, yield 37.8%. M.p.: 167.4–169.2 °C. ^1H NMR (400 MHz, CDCl_3) $\delta = 10.05$ (t, $J = 4.7$ Hz, 1H), 9.43 (d, $J = 1.8$ Hz, 1H), 8.99–8.85 (m, 2H), 8.35–8.24 (m, 2H), 7.76–7.51 (m, 6H), 7.07 (d, $J = 9.2$ Hz, 2H), 6.90–6.82 (m, 1H), 6.71 (t, $J = 8.4$ Hz, 1H), 6.48 (d, $J = 8.8$ Hz, 2H), 4.30–4.10 (m, 4H), 3.52 (t, $J = 5.6$ Hz, 2H), 2.09–1.90 (m, 2H), 1.85–1.73 (m, 1H), 1.46–1.25 (m, 28H), 1.03–0.87 (m, 14H). MALDI-HRMS: calcd ($[\text{C}_{60}\text{H}_{70}\text{N}_7\text{O}_4\text{Pt}+\text{H}]^+$): $m/z = 1147.5137$, found $m/z = 1147.5057$.

Nanosecond Time-Resolved Transient Difference Absorption Spectroscopy. Nanosecond time-resolved transient difference absorption spectra were recorded on a LP 920 laser flash photolysis spectrometer (Edinburgh Instruments, Livingston, UK). The samples were purged with N_2 or argon for 30 min before measurement. The samples were excited with a nanosecond pulsed laser (Vibrant 355II, wavelength tunable in the range of 410 – 2400 nm), and the transient signals were recorded on a Tektronix TDS 3012B oscilloscope.

TTA Upconversion. Diode-pumped solid state laser was used for upconversions (445 nm). The laser power was measured with a phototube. The mixed solution of the Pt(II) complex (triplet photosensitizer) and DPA (triplet acceptor) was degassed for at least 15 min with N_2 or argon before measurement. The spectra were recorded on a adapted RF5301PC spectrofluorometer

(Shimadzu, Japan).

The Delayed Fluorescence of the Upconversion (τ_{DF}). The delayed fluorescence (τ_{DF}) was measured with OpoletteTM 355II+UV nanosecond pulsed laser (typical pulse length: 7 ns. Pulse repetition: 20 Hz. Peak OPO energy: 4 mJ. Wavelength is tunable in the range of 210 – 355 nm and 410 – 2200 nm. OPOTEK, USA), which is synchronized to FLS 920 spectrofluorometer (Edinburgh, UK). The decay kinetics of the upconverted fluorescence (delayed fluorescence) was monitored with FLS920 spectrofluorometer. The prompt fluorescence lifetime of the triplet acceptor perylene was measured with EPL picosecond pulsed laser (405 nm) which is synchronized to the FLS 920 spectrofluorometer.

Theoretical Calculations. DFT calculations with B3LYP/6-31G/LANL2DZ basis set were used for optimization of both the ground-state and triplet states. The energy levels of the T_1 states (energy gap between S_0 and T_1) were calculated with time-dependent DFT (TDDFT) on the basis of optimized triplet state geometries. All the calculations were carried out with Gaussian 09W.²⁹

Results and discussion

Molecules Design and Synthesis.

The $\text{C}^{\wedge}\text{N}^{\wedge}\text{N}$ ligand and the $\text{C}^*\text{N}^{\wedge}\text{N}$ ligand with different redox potential properties were selected to form Pt(II) coordination center **Pt-a** and **Pt-b**, respectively. Recently it was reported that the coordination geometry of **Pt-a** is a perfect planar square structure,²⁷ thus photoluminescence efficiency based on **Pt-a** is high. However, photoredox properties (driving forces for charge transfer) and their energy levels of emission and absorption (driving forces for energy transfer) also play important roles for the photoluminescence efficiency. Introducing different aryl-acetylide ligands would have substantial influence on the properties mentioned above, further affect the photoluminescent efficiency. In order to study the synergetic effect of the arylacetylide ligands and $\text{C}^{\wedge}\text{N}^{\wedge}\text{N}/\text{C}^*\text{N}^{\wedge}\text{N}$ Pt cooperation center on the photoredox and photophysical properties of the complexes, Py was selected as the ligand. It was reported that complexes with pyrenyl acetylide ligands gave long-lived triplet excited state.^{28,30} However, the corresponding Pt(II) complexes (**Pt-1** and **Pt-2**) were not stable. Therefore, NI and NDI acetylide ligands with strong electron withdrawing ability were used as ligands to enhance the stability of Pt(II) complexes. Herein these aryl-acetylide ligands were used for investigation of the effect of $\text{C}^{\wedge}\text{N}^{\wedge}\text{N}/\text{C}^*\text{N}^{\wedge}\text{N}$ ligands and acetylides on the photoredox and photophysical properties of the Pt(II) complexes. The synthesis procedure is based on the routine methods. All the complexes were obtained with moderate to satisfactory yields.

Electrochemical data of the complexes.

The electrochemical properties of the ligands and complexes were studied with cyclic voltammetry (Fig. 1). For complex **Pt-a**, oxidation waves at +0.6 V and +1.01 V were observed, which could be assigned to the $\text{C}^{\wedge}\text{N}^{\wedge}\text{N}$ Pt(II) coordination center. No reduction wave was found. These results indicate the possibility

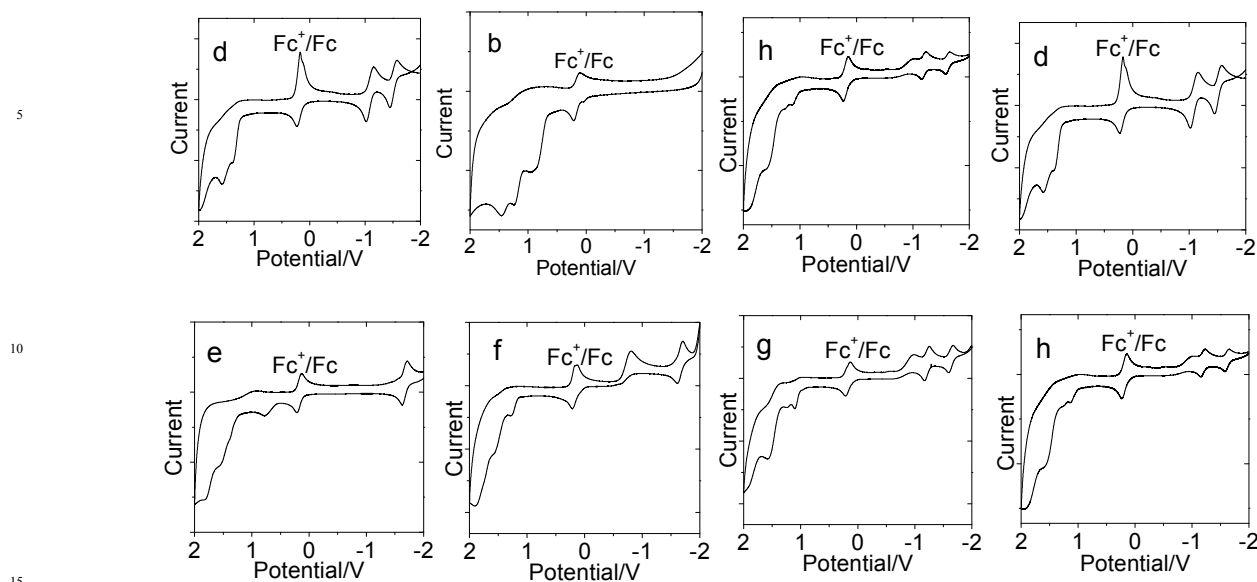


Fig. 1 Cyclic voltammogram of (a) **Pt-a**, (b) **Pt-b**, (c) **L-2**, (d) **L-3**, (e) **Pt-3**, (f) **Pt-4**, (g) **Pt-5** (h) **Pt-6**. In deaerated CH_2Cl_2 solutions containing 1.0 mM photosensitizers with the ferrocene, 0.10 M Bu_4NPF_6 as supporting electrolyte, Ag/AgNO_3 reference electrode, Scan rates: 50 mV/s. Ferrocene (Fc) was used as internal reference.

of the charge transfer from $\text{C}^*\text{N}^*\text{N}$ Pt(II) coordination center to arylacetylide ligand (MLCT). For **Pt-b**, a few oxidation waves at +0.91 V, +1.17 V and +1.39 V were observed, wherein oxidation waves at +1.17 V could be assigned to the structure of N,N -diphenyl pyridineamine in the $\text{C}^*\text{N}^*\text{N}$ Pt(II) coordination center.³¹ Other two waves at +0.91 V and +1.39 V could be assigned to $\text{C}^*\text{N}^*\text{N}$ Pt(II) coordination center. The use of aniline linker breaks the π conjugation of $\text{C}^*\text{N}^*\text{N}$ Pt(II) coordination center, resulting in obviously positive shift (above 0.30 V). For the ethynyl Ni ligand (**L-2**), a reduction wave at -1.45 V was observed, indicating that **L-2** is a good electron acceptor. For NDI acetylide ligand (**L-3**), two reversible reduction waves at -1.02 V and -1.45 V were observed. For **Pt-3** with Ni acetylide ligand (electron withdrawing substitute), the reduction wave at -1.62 V and the oxidation wave at 1.51 V was observed, which can be assigned to the Ni acetylide ligand. The oxidation wave at +0.77 V was observed and can be assigned to $\text{C}^*\text{N}^*\text{N}$ Pt(II) coordination center. Compared with **Pt-a**, the oxidation potential of **Pt-3** shows 0.17 V positive shift, indicating perturbation of the electronic structure of the Ni ligand. At the same time, the more positive oxidation potential enhances the stability of Pt(II) complexes.³² On the other hand, no reversible reduction wave was observed, which is different from **Pt-a**, indicating that the coordination of Ni acetylide ligand to the Pt(II) center impose substantial influence on the electronic structure of the $\text{C}^*\text{N}^*\text{N}$ Pt(II) coordination center. For **Pt-4**, the onset oxidation wave was observed at +1.27 V. Compared with **Pt-b**, **Pt-4** shows 0.36 V positive shift, indicating that the electronic structure of the Ni ligand is substantially altered upon coordination to Pt(II) atom. Thus the effects of the $\text{C}^*\text{N}^*\text{N}$ or the $\text{C}^*\text{N}^*\text{N}$ ligand are different. Similar results were also observed for **Pt-5** and **Pt-6**. The electrochemical data of the complexes and the ligands were listed in Table 1. Complexes **Pt-1** and **Pt-2** with Py ligand are unstable, thus the CV data were

not collected.

In order to further investigate charge transfer process (MLCT), the thermodynamic driving forces for charge transfer process (ΔG^0 , free energy change of the potential charge transfer) were calculated based on the redox potential values, by employing the Rehm-Weller Equation (Eq. 1).³³

$$\Delta G^0 = E_{\text{ox}} - E_{\text{red}} - E_{0,0} - C \quad \text{Eq. (1)}$$

wherein ΔG^0 is the free energy changes of the potential charge transfer. E_{ox} is oxidation potential of the electron donor (Pt coordination center), E_{red} is reduction potential of the electron acceptor (acetylid ligand), $E_{0,0}$ is excitation energy, which is calculated based on the wavelength of maximum absorption in the visible region, C could be regarded as a constant, which is related to the solvents. These measurements were operated under the same solvent, so C could be ignored [Eq. (1)].

Pt-3 shows more negative ΔG^0 (-0.7 eV) than others, indicating that charge transfer process is enhanced (see Table 1 and ESI †). **Pt-3** has the lower phosphorescence quantum yield (vide infra). For **Pt-4**, the more positive onset oxidation potential (1.27 V) contributes to the increase of ΔG^0 (0.00 eV), as **Pt-4** shows significantly higher ΔG^0 than that of **Pt-3**, which means much weaker ability to undergo charge transfer process thermodynamically. The phosphorescence quantum yield of **Pt-4** is enhanced ($\Phi_p = 0.14$). Although the ΔG^0 of **Pt-5** (0.04 eV) is higher than that of **Pt-4** (0.00 eV), the phosphorescence quantum yield of **Pt-5** is still lower than that of **Pt-4** ($\Phi_p = 0.14$). Therefore, energy level also need to be considered for the design of Pt(II) complexes (vide infra).

Table 1. Electrochemical data of Pt-a, Pt-b, L-2, L-3, Pt-3, Pt-4, Pt-5 and Pt-6.

Compd	Oxidation (V) ^a			Reduction (V) ^a		ΔG°
	I	II	III	I	II	
Pt-a	+0.60	+1.01	– ^b	– ^b	– ^b	– ^b
Pt-b	+0.91	+1.17	+1.39	– ^b	– ^b	– ^b
L-2	+1.53	– ^b	– ^b	–1.45	– ^b	– ^b
L-3	+1.57	– ^b	– ^b	–1.02	–1.45	– ^b
Pt-3	+0.77	+1.51	– ^b	–1.62	– ^b	–0.73
Pt-4	+1.27	+1.55	– ^b	–1.61	– ^b	+0.00
Pt-5	+1.10	+1.58	– ^b	–1.16	–1.59	+0.04
Pt-6	+1.12	+1.57	– ^b	–1.15	–1.59	–0.05

^a Recorded with [Bu₄N][PF₆] as the electrolyte in CH₂Cl₂ (0.1 M) at ambient temperature with a scan rate of 50 mV/s. Potentials are expressed as the half-wave potentials ($E_{1/2}$) in volts vs Ag/AgNO₃ using ferrocene as an internal reference. ^b Not determined. ^c free energy changes of the potential PET effect with Rehm–Weller Equation.

Steady state UV–Vis absorption and luminescence emission spectroscopy

The absorption spectra of Pt-a and Pt-b are shown in Fig. 2a. The spectra show strong absorptions in the high-energy region and weaker absorptions in the low-energy region. The high-energy absorptions can be assigned as ligand based $\pi\text{-}\pi^*$ transitions, while the low energy absorptions can be assigned as charge transfer bands.²⁷ The $S_0 \rightarrow {}^1\text{MLCT}$ absorption bands in parent complexes Pt-a and Pt-b were observed at 390 nm and 419 nm, respectively. The UV–Vis absorption spectra of the ligands were studied (see ESI †). L-1 gives absorption in the UV region. The molar absorption coefficient (ϵ) is $4.92 \times 10^4 \text{ M}^{-1} \text{ cm}^{-1}$ at 360 nm. The intense structured absorption of the pyrenylacetylide was reduced in the complexes Pt-1 and Pt-2 (Fig. 2b). Moreover, the absorption intensity was reduced as compared with that of the free ligands. These results indicated that the π -conjugation framework of L-1 is substantially perturbed in the complexes Pt-1 and Pt-2. This is reasonable since the Pt(II) atom is the linker to the pyrenyl moiety by the C≡C triple bond.³⁴ Similar results were observed for Pt-3 and Pt-4 (Fig. 2c). Moreover, the maximal absorption wavelength of the complexes Pt-3 and Pt-4 are much red-shifted as compared with that of ligand L-2. Based on the DFT/TDDFT calculations, the intense absorption of Pt-3 at 397 nm could be attributed to the mixed ${}^1\text{MLCT}$ and ${}^1\text{IL}$ excited states (see ESI †). These results are in accordance with photoredox properties ($\Delta G^\circ = -0.73 \text{ eV}$). The absorption of Pt-4 at 431 nm could be attributed to the energy level of the ${}^1\text{IL}$ excited state. The photoredox properties ($\Delta G^\circ = 0.00 \text{ eV}$) and DFT/TDDFT

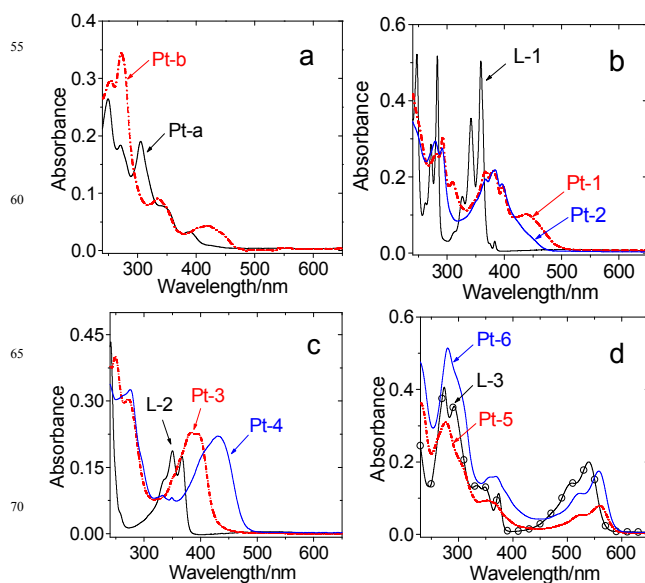


Fig. 2 UV–Vis absorption of (a) Pt-a and Pt-b; (b) L-1, Pt-1 and Pt-2; (c) L-2, Pt-3 and Pt-4; (d) L-3, Pt-5 and Pt-6. $c = 1.0 \times 10^{-5} \text{ M}$ in dichloromethane (DCM), 20 °C.

calculations (Table 3) also confirmed that Pt-4 show less MLCT character than that of Pt-3. Pt-5 and Pt-6 show similar absorption wavelength as compared with that of the ligand L-3 (Fig. 2d). The absorption of Pt-5 and Pt-6 at around 559 nm could be attributed to their ${}^1\text{IL}$ excited states. These results are also confirmed by the DFT/TDDFT calculations (see ESI †).

The UV-Vis absorption spectra of the ligands and the complexes in different solvents were studied. The low energy absorptions of **Pt-3** showed a little solvent dependence and shifted to the higher energy by up to 23 nm as the solvents switch from toluene to MeOH, indicating that these low energy transitions possess, to some extent, charge transfer character. No significant changes were observed for **Pt-4**, **Pt-5** and **Pt-6** (see ESI †), indicating that these absorption could be attributed to ^1IL excited state.

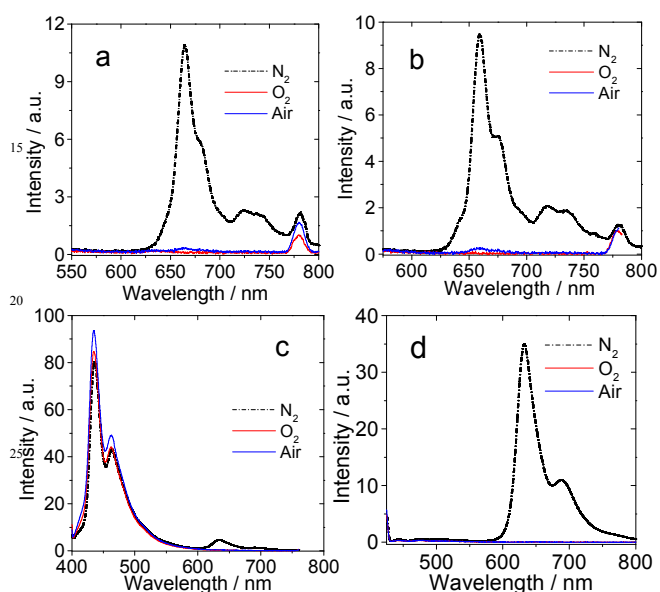


Fig. 3 The emission spectra of the Pt(II) complexes under different atmosphere. (a) **Pt-1** ($\lambda_{\text{ex}} = 390$ nm); (b) **Pt-2** ($\lambda_{\text{ex}} = 390$ nm); (c) **Pt-3** ($\lambda_{\text{ex}} = 390$ nm); (d) **Pt-4** ($\lambda_{\text{ex}} = 420$ nm). $c = 1.0 \times 10^{-5}$ M in toluene, 20 °C.

The photoluminescence of the complexes were studied (Fig. 3a and 3b). For complexes **Pt-1** and **Pt-2**, strong emission at 660 nm was observed, which are highly sensitive to O_2 . The emission can be completely quenched in aerated solution. Thus the emission is due to emissive triplet excited states. This postulation is in agreement with the previous observation of phosphorescence with pyrenylacetylde Pt(II) complexes.¹⁵

Interestingly, the emission property of **Pt-3** and **Pt-4** was drastically different. For **Pt-3** (Fig. 3c), the major emission band is centered at 434 nm, for which the emission intensity is independent on the atmosphere (air or O_2), thus the emission band at 434 nm can be assigned as fluorescence. Moreover, a minor emission band at 629 nm was observed, which can be quenched by O_2 . Thus the emission band can be assigned as phosphorescence. The emission band at 434 nm is not due to any impurity of free ligand in the complex, because the emission wavelength is much longer than that of the ligand **L-2**. The different emission property of **Pt-3** and **Pt-4** can be rationalized by the different influence of the ligands, demonstrated by the cyclic voltametry study as well as the UV-Vis absorption spectra of the complexes **Pt-3** and **Pt-4**. The ΔG° value of **Pt-4** is 0.00 eV, which shows a good balance for the energy transfer and charge transfer. The phosphorescence emission of **Pt-4** is assigned to ^3IL (vide infra). The phosphorescence quantum yield is up to 0.14, which is higher than other complexes. In order to

study the triplet state yields of the complexes, the photosensitization of singlet oxygen ($^1\text{O}_2$) with the complexes upon photoexcitation was studied and the $^1\text{O}_2$ quantum yields (Φ_Δ) were determined (Table 2). The $^1\text{O}_2$ quantum yields (Φ_Δ) with **Pt-4** as triplet photosensitizers was determined as 0.65, indicating efficient intersystem crossing (ISC).

The ΔG° value of the electron transfer in **Pt-3** was calculated as -0.7 eV. The singlet oxygen quantum yield of **Pt-3** is 0.57, indicating efficient intersystem crossing.

The emission of **Pt-5** and **Pt-6** are centered at 570 nm, which are not dependent on the atmosphere of the solution, thus the emission bands can be assigned as fluorescence (see ESI †). Similar to **Pt-1**, the emission bands of **Pt-5** and **Pt-6** are different from that of the free ligand **L-3**, thus the emission band of **Pt-5** and **Pt-6** are not due to the un-coordinated free ligand. At the same time, the energy level of ^1IL state (2.22 eV) is much lower than that of $^1\text{MLCT}$ state (3.02 eV), so the $^1\text{IL} \rightarrow ^1\text{MLCT}$ process is inhibited. These reasons cause the non-phosphorescence. The singlet oxygen quantum yield of **Pt-5** ($\Phi_\Delta = 0.07$) also infers the poor triplet state yield, which confirm the results mentioned above and not the limits of detection range of the spectrophotometer.

The ΔG° value of **Pt-6** is -0.05 eV. Due to the weak charge transfer impetus (low ΔG° value), the charge transfer process from Pt(II) coordination center to NDI ligand is inefficient. **Pt-6** show no phosphorescence and the singlet oxygen quantum yield of **Pt-6** is 0.09.

In order to clarify the electronic feature of the emissive triplet excited state of the complexes, i.e. as $^3\text{MLCT}$ state or ^3IL state, the emission spectra of **Pt-4** at 77 K was compared with that at RT (Fig. 4). The emission band at 77 K is slightly blue-shifted as compared with that at RT. The thermally induced Stokes shift is 245 cm^{-1} . The emission band at 77 K is more structured than that at RT. Thus the emissive triplet excited state of **Pt-4** can be assigned as ^3IL state, otherwise more significant thermally induced Stokes shift will be observed.

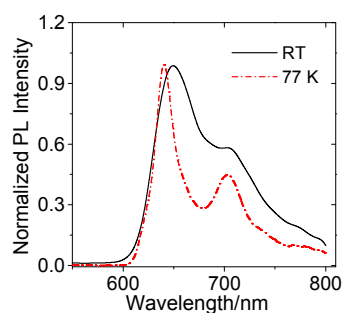


Fig. 4 Photoluminescence spectra of **Pt-4** at room temperature (RT) and 77 K ($\lambda_{\text{ex}} = 425$ nm). $c = 2.0 \times 10^{-5}$ M in mixed solvent $\text{C}_2\text{H}_5\text{OH}-\text{CH}_3\text{OH}$ (4 : 1, v/v).

110 Nanosecond time-resolved transient difference absorption spectroscopy

In order to study the triplet excited state of the complexes, nanosecond time-resolved transient difference absorption spectra of the complexes were investigated (Fig. 5).⁹ For **Pt-4**, a bleaching band at 430 nm was observed upon excitation with

450 nm nanosecond pulsed laser. Moreover, strong transient absorption band in the region of 470 nm – 740 nm was observed, which can be assigned as the absorption of T_1 state ($T_1 \rightarrow T_n$ transitions).²⁵ The lifetime was determined as 90.1 μ s (at $c = 1.0 \times 10^{-5}$ M). The triplet state lifetime is long, thus triplet-triplet annihilation of **Pt-4** has to be considered, with which the lifetime can be reduced at high concentration. Therefore the triplet state lifetime of the complex was measured at lower concentration; the intrinsic triplet state lifetime of **Pt-4** was extrapolated as 126.7 μ s (in infinite diluted solution. see ESI†).

No transient spectra can be observed for **Pt-5** and **Pt-6** under photoexcitation at 555 nm and 560 nm respectively, which may be due to the poor triplet quantum yield. Since **Pt-1** and **Pt-2** are not stable, no transient absorption spectra were recorded for these two complexes.

DFT calculations

The ground state geometries of the complexes were optimized using DFT methods. For **Pt-4** (Fig. 6 and Table 3), the UV-Vis absorption of **Pt-4** was calculated based on the optimized ground state geometry. The absorption band in the visible region was predicted at 459 nm, which is close to the experimental result of 431 nm (Fig. 3b). It is known that the DFT methods usually underestimate the excitation energy for charge transfer transitions. The electronic components of the $S_0 \rightarrow S_1$ transition are H \rightarrow L, which can be assigned as the IL and MLCT mixed transition, with IL as the major component. The singlet-triplet state energy gaps were also calculated. The energy level of the T_1 state was estimated to be 1.93 eV (642

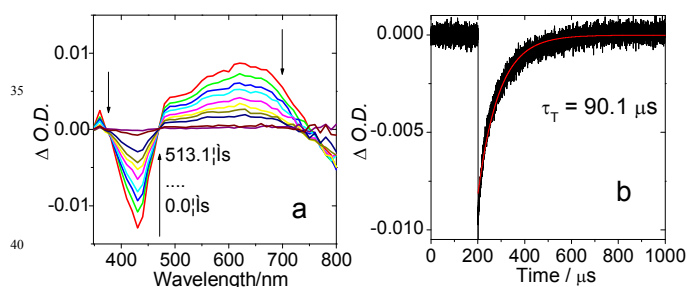


Fig. 5 Nanosecond time-resolved transient difference absorption spectra of (a) **Pt-4** after pulsed excitation ($\lambda_{ex} = 430$ nm). (b) Decay traces of **Pt-4** at 450 nm. $c = 1.0 \times 10^{-5}$ M in deaerated toluene, 25 $^{\circ}$ C.

nm). H \rightarrow L is involved in the T_1 state, thus the T_1 state can be assigned as the 3 IL state, which is in agreement with the spin density analysis and the long lived triplet excited state observed for **Pt-4**. The geometry of **Pt-3**, **Pt-5** and **Pt-6** were also optimized. The calculated absorption is close to the experimental observations (see ESI†).

To assign the triplet states of the complexes, the spin density surfaces were calculated by DFT methods.^{35–37} For **Pt-a** and **Pt-b**, the spin density surfaces are located in the tridentate ligand and Pt(II) coordination centers, which could be assigned as 3 MLCT states (Fig. 7). The triplet excited states of the Pt(II) complexes are localized on the acetylide ligands. It is in agreement with the long-lived triplet excited states of the complexes.

Table 2. Photophysical parameters of **Pt-1** – **Pt-6**, **L-1**, **L-2** and **L-3**.

	λ_{abs}^a	ϵ^b	λ_{em}^c	Φ_F	Φ_P	τ_F (ns) ^g		τ_P (μ s) ^h		τ_T/μ s ⁱ	Φ_{Δ}^j
						298 K	298 K	77 K	77 K		
Pt-1	400	1.61	663	– ^k	0.9% ^f	– ^k	– ^k	– ^k	– ^k	– ^k	– ^k
Pt-2	398	2.06	659	– ^k	3.6% ^f	– ^k	– ^k	– ^k	– ^k	– ^k	– ^k
Pt-3	397	2.48	434\629	5.7% ^f	0.6% ^f	4.50	30.6	– ^k	– ^k	– ^k	0.57
Pt-4	431	2.26	631	– ^k	14.4% ^f	– ^k	– ^k	137.0	90.1	90.1	0.65
Pt-5	559	0.88	564	3.5% ^d	– ^k	9.69	– ^k	250.9	– ^k	– ^k	0.07
Pt-6	558	1.69	582	0.6% ^d	– ^k	9.37	– ^k	– ^k	– ^k	– ^k	0.09
L-1	360	4.92	384\404	8.9% ^e	– ^k	3.32	– ^k	– ^k	– ^k	– ^k	– ^k
L-2	350	1.74	400	7.6% ^e	– ^k	2.21	– ^k	– ^k	– ^k	– ^k	– ^k
L-3	536	1.98	561	16.9% ^e	– ^k	11.43	– ^k	– ^k	– ^k	– ^k	– ^k

^a In toluene (1.0×10^{-5} mol/dm³). ^b Molar extinction coefficient at the absorption maxima. $\epsilon: 10^4$ /cm² mol⁻¹ dm³. ^c In toluene ^d In toluene, with 2,6-diiodo-^e Bodipy ($\Phi = 0.027$ in acetonitrile) as the standards. ^e In toluene, with quinone sulfate ($\Phi = 0.546$ in 0.5 M H₂SO₄) as the standards. ^f In toluene, with [Ru(dmb)₃(PF₆)₂] ($\Phi = 0.073$ in acetonitrile) as the standards. ^g Luminescence lifetime, **Pt-3** ($\lambda_{ex} = 443$ nm), **Pt-5** and **Pt-6** ($\lambda_{ex} = 473$ nm) at RT. ^h Phosphorescence lifetime, **Pt-3** ($\lambda_{ex} = 397$ nm) and **Pt-4** ($\lambda_{ex} = 431$ nm) at RT. ⁱ Triplet state lifetimes, measured by nanosecond transient difference absorption spectroscopy. ^j Quantum yield of singlet oxygen (1O_2), For **Pt-3** and **Pt-4**, [Ru(bpy)₃(PF₆)₂] was used as standard ($\Phi_{\Delta} = 0.57$ in acetonitrile), For **Pt-5** and **Pt-6**, 2,6-diiodo-Bodipy was used as standard ($\Phi_{\Delta} = 0.79$ in CH₂Cl₂), $c = 1.0 \times 10^{-5}$ M in acetonitrile. ^k Not applicable.

70

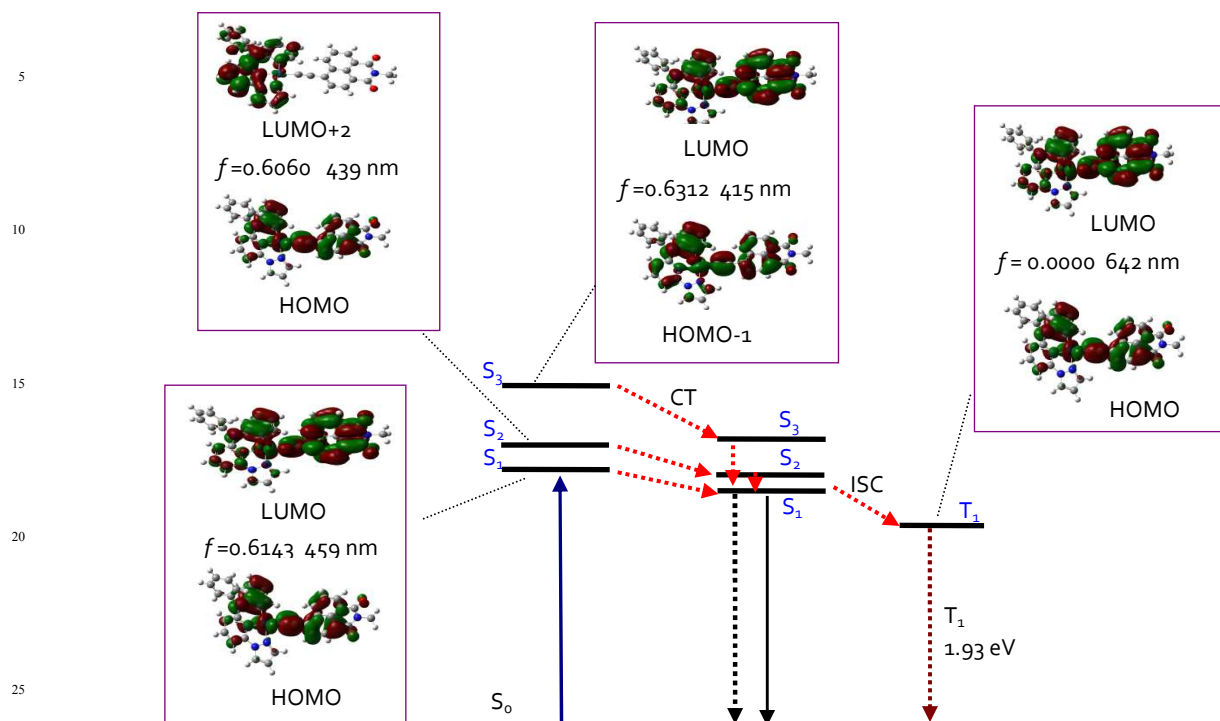


Fig. 6 Selected frontier molecular orbitals involved in the excitation and the singlet/triplet excited states of **Pt-4**. CT stands for conformation transformation. The left column is UV-Vis absorption (based on the ground state geometry) and the right column is the triplet excited state (based on the ground state geometry). For clarity, only the selected excited states were presented. The calculations are at the B₃LYP/6-31G/LANL2DZ level using Gaussian 09W.

Table 3. Selected electronic excitation energies (eV) and corresponding oscillator strengths (*f*), main configurations and CI coefficients of the low-lying electronically excited states of **Pt-4**. Based on the optimized ground state geometries, the calculations are at the B₃LYP/6-31G/LANL2DZ level using Gaussian 09W.

Pt-4	Electronic transition	TDDFT//B ₃ LYP/6-31G				
		Energy(eV) ^a	<i>f</i> ^b	Composition ^c	CI ^d	Character
Singlet	S ₀ →S ₁	2.70 eV/459 nm	0.3550	H→L	0.6143	ILCT
				H→L+1	0.3102	ILCT
	S ₀ →S ₂	2.82 eV/439 nm	0.0896	H-1→L+1	0.1364	MLCT, ILCT
				H→L	0.3016	ILCT
				H→L+2	0.6060	ILCT
S ₀ →S ₃	2.99 eV/415 nm	0.2449	H-1→L	0.6312	MLCT, ILCT	
S ₀ →S ₄	3.10 eV/401 nm	0.0961	H-1→L+1	0.6351	MLCT, ILCT	
Triplet	S ₀ →T ₁	1.93 eV/642 nm	0.0000	H→L	0.5094	ILCT
				H-1→L	0.4382	MLCT, ILCT
	S ₀ →T ₂	2.57 eV/483 nm	0.0000	H→L+1	0.5226	ILCT
	S ₀ →T ₃	2.77 eV/447 nm	0.0000	H-1→L	0.4069	MLCT, ILCT
				H→L	0.4102	ILCT

^a Only selected excited states were considered. The numbers in parentheses are the excitation energy in wavelength. ^b Oscillator strength. ^c H stands for HOMO and L stands for LUMO. Only the main configurations are presented. ^d Coefficient of the wave function for each excitations. The CI coefficients are in absolute values.

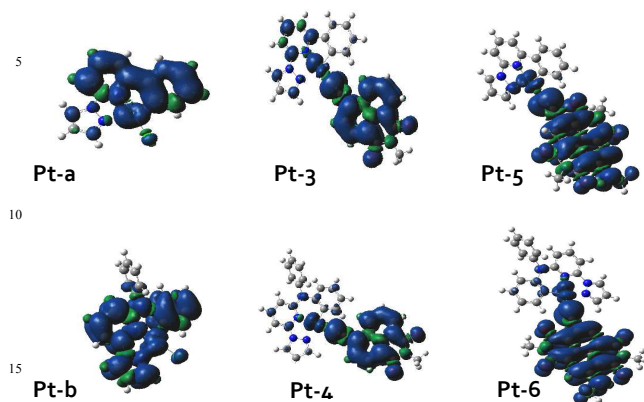


Fig. 7 Spin density of the complexes **Pt-a**, **Pt-b**, **Pt-3** - **Pt-6** at the optimized triplet state geometries. Toluene was used as the solvent in the calculations. Calculation was performed at B₃LYP/6-31G/LANL2DZ level with Gaussian 09W.

Triplet-triplet annihilation upconversion

Triplet-triplet annihilation (TTA) upconversion has attracted much attention due to the advantages of low excitation light power threshold, high upconversion quantum yields, and tunable excitation/emission wavelength.^{38,39} Triplet photosensitizer is crucial for TTA upconversion.⁴⁰ Thus, it is important to develop new triplet photosensitizers for TTA upconversion. To the best of our knowledge, very few tridentate cyclometalated Pt(II) acetylide complexes have been used as triplet photosensitizers for TTA upconversion.^[28,35] Herein the Pt(II) complexes were used for TTA upconversion. **Pt-4** shows strong absorption of visible light and long-lived triplet excited state, TTA upconversion with **Pt-4** as triplet photosensitizer was studied (Fig. 8). Upon 445 nm laser excitation, phosphorescence band at 634 nm was observed. A triplet acceptor is an essential component for TTA upconversion.^{8,9} One of the prerequisites for a useful triplet photosensitizer is that the energy level of the T₁ state of a triplet acceptor must be lower than the energy level of the T₁ state of the photosensitizer.

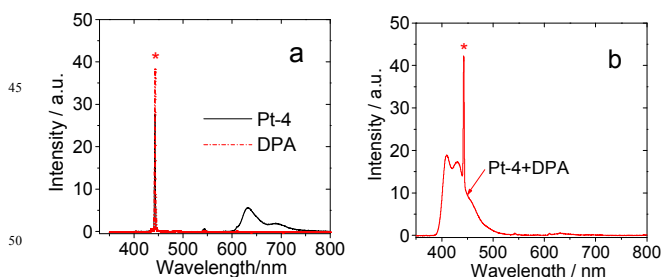


Fig. 8 Emission and upconversion of the complexes with 445 nm (5.2 mW) laser excitation. (a) Emission of the complexes alone. (b) The upconverted DPA fluorescence and the residual fluorescence and phosphorescence of **Pt-4**. The asterisks in (a) and (b) indicate the scattered 445 nm excitation laser (5.2 mW). c [DPA] = 4.0 × 10⁻⁵ M; c [sensitizers] = 1.0 × 10⁻⁵ M in deaerated toluene, 25 °C.

Based on the T₁ state energy level of **Pt-4** (λ_{em} = 631 nm, 1.97 eV), 9,10-diphenylanthracene (DPA) was selected as the triplet acceptor (T₁ state energy level is 1.77 eV). In the presence of triplet acceptor, strong emission in the region of 400–500 nm was observed. This is due to the upconverted fluorescence emission of DPA. Excitation of DPA alone at 445 nm did not give any emission in the region of 400–500 nm, thus the TTA upconversion with **Pt-4**/DPA is verified. The triplet-triplet annihilation upconversion and upconversion quantum yield was determined as 29.7%, which is very high for TTA upconversion.^{8,9}

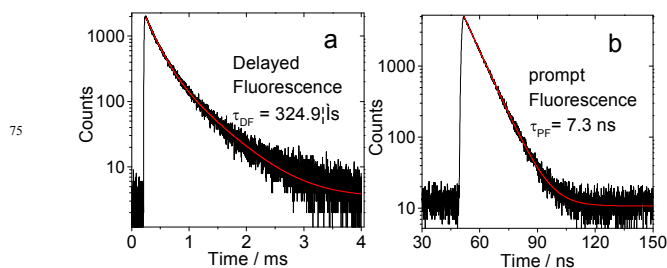


Fig. 9 Delayed fluorescence observed in the TTA upconversion with (a) **Pt-4** as the triplet photosensitizer and DPA as the triplet acceptor. Excited at 440 nm and monitored at 410 nm. (b) The prompt fluorescence decay of DPA determined in a different experiment (excited with picosecond 405 nm laser, the decay of the emission was monitored at 410 nm). c [DPA] = 4.0 × 10⁻⁵ M; c [sensitizers] = 1.0 × 10⁻⁵ M in deaerated toluene, 25 °C.

In order to confirm the TTA upconversion, the luminescence lifetime of the TTA upconversion emission was determined (Fig. 9). The luminescence lifetime was determined as 324.9 μs. On the contrary, the luminescence lifetime of the prompt fluorescence of DPA was determined as 7.3 ns. Thus the TTA upconversion is proved.

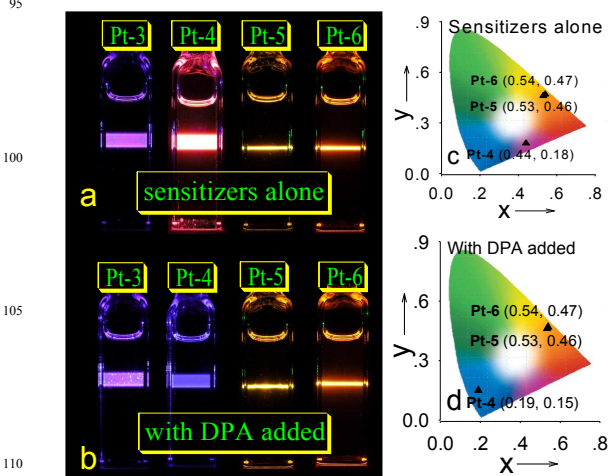


Fig. 10 Photographs of the emission of (a) sensitizers alone and (b) the upconversion. CIE diagram of the emission of (c) sensitizers alone and (d) in the presence of DPA (upconversion). (For **Pt-3** and **Pt-4**, λ_{ex} = 445 nm, **Pt-5** and **Pt-6**, λ_{ex} = 532 nm) (laser power: 5.2 mW). c [sensitizer] = 1.0 × 10⁻⁵ M, c [DPA] = 4.0 × 10⁻⁵ M in deaerated toluene, 25 °C.

The photographs of the luminescence of the sensitizers alone and the upconversion are shown in Fig. 10. The upconversion with **Pt-4** as the triplet photosensitizer is clearly visible to the unaided eyes. **Pt-4** alone gives red emission, while the mixed solution of **Pt-4** and DPA shows a purple emission. However, the emission wavelength of the **Pt-3** solution does not change in the presence of DPA, indicating the lack of TTA upconversion for **Pt-3**, which is due to its poor absorption ability at 445 nm. For **Pt-5** and **Pt-6**, no upconverted blue emission was observed, which attributes to low quantum yield of triplet excited state. The change in the emission color of the triplet photosensitizers with and without the triplet acceptor DPA were quantified with the CIE coordinates. For **Pt-4**, the CIE coordinates change from (0.44, 0.18) to (0.19, 0.15). For **Pt-5** and **Pt-6**, no significant change was observed.

In order to study the efficiency of the triplet-triplet-energy transfer (TTET) process, which is crucial for the TTA upconversion, the quenching of the triplet state of the photosensitizers was measured using nanosecond transient absorption (see ESI †). Significant quenching was observed for **Pt-4**, with quenching constants of $5.65 \times 10^5 \text{ M}^{-1}$ (see ESI †). In order to unambiguously confirm the TTA upconversion is responsible for the blue emission band of the triplet photosensitizer/DPA mixed samples, the time-resolved emission spectra (TRES) were also recorded (Fig. 11). For **Pt-4** alone, long-lived emission in the region of 631 nm was observed (Fig. 11a), with lifetime of 55.21 μs . The difference between the lifetime values and that determined in the previous section (Table 1) is due to the fact that the background dynamics of the pulsed laser cannot be calibrated in the TRES mode. For the mixture of **Pt-4**/DPA, however, the emission band in the region 631 nm was quenched, a new emission band in the 420 nm

region developed (Fig. 11b). The lifetime of the emission is 324.9 μs . This long-lived fluorescence emission is the characteristic feature of the TTA upconversion.

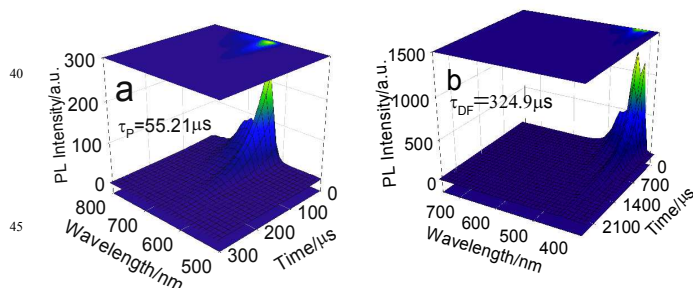
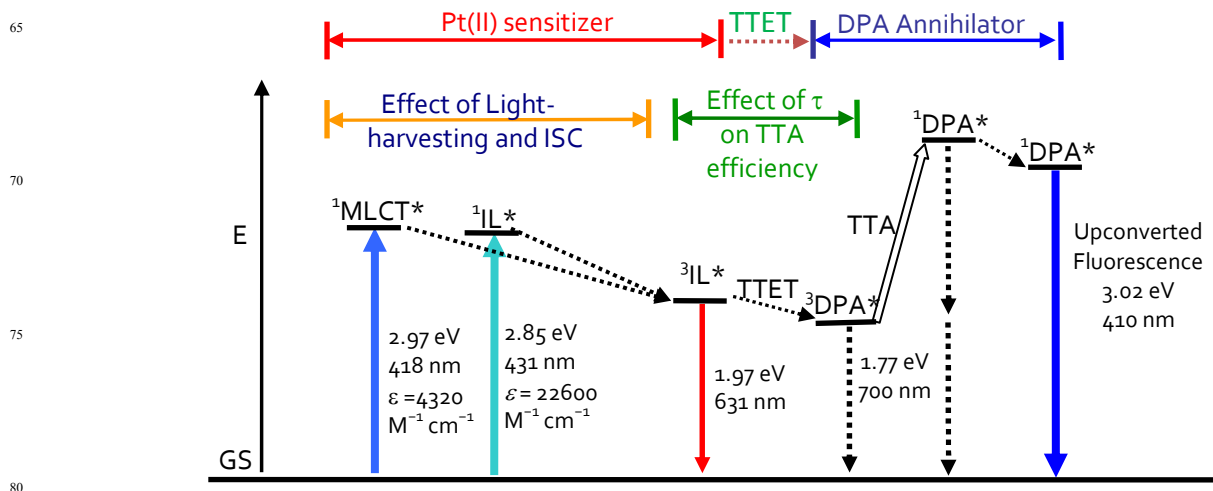


Fig. 11 Time-resolved emission spectra (TRES) of **Pt-4** alone and the TTA upconversion with the DPA as the triplet acceptor. **Pt-4** alone: (a) the phosphorescence region was measured (550 nm–800 nm, $\tau = 55.2 \mu\text{s}$) excited with nanosecond pulsed OPO laser (440 nm). TRES of **Pt-4** in the presence of DPA: (b) upconverted emission in the range of 400 nm–500 nm was observed ($\tau = 324.9 \mu\text{s}$) with nanosecond pulsed OPO laser (440 nm). $c[\text{DPA}] = 4.0 \times 10^{-5} \text{ M}$; $c[\text{sensitizers}] = 1.0 \times 10^{-5} \text{ M}$ in deaerated toluene, 25 °C.

The TTA upconversion process can be summarized in Scheme 2. Firstly the singlet excited state of the triplet sensitizers are populated upon photoexcitation. Direct excitation of the ligand (^1IL) or $^1\text{MLCT}$ will both lead to the population of singlet excited state. With the heavy atom effect of the Pt(II) atoms, the $S_1 \rightarrow T_1$ ISC will lead to ^3IL excited state. Note that the ^3IL excited state shows a much longer lifetime



Scheme 2. Jablonski diagram of triplet-triplet-annihilation (TTA) upconversion with **Pt-4** as a triplet sensitizer (the triplet states of sensitizers are emissive) and 9,10-diphenylanthracene (DPA) was the triplet acceptor. E is energy. GS is ground state (S_0). $^3\text{IL}^*$ is intraligand triplet excited state (NI localized). TTET is triplet-triplet energy transfer. $^3\text{DPA}^*$ is the triplet excited state of DPA. TTA is triplet-triplet annihilation. $^1\text{DPA}^*$ is the singlet excited state of DPA. The emission bands observed for the sensitizers alone is the $^3\text{IL}^*$ emissive excited state. The emission bands observed in the TTA experiment is the simultaneous $^3\text{IL}^*$ emission (phosphorescence) and the $^1\text{DPA}^*$ emission (fluorescence).

than the normal $^3\text{MLCT}$ state. Thus the efficiency of TTEP process will be improved. Annihilation of the triplet excited state of the triplet acceptor (DPA) will produce the singlet excited state and as a result the singlet emission (delayed fluorescence) will be observed. The wavelength of upconverted fluorescence is shorter than the initial photo-excitation wavelength. It should be pointed out that the long-lived ^3IL triplet excited state of **Pt-4** makes it an ideal triplet photosensitizer for triplet-triplet annihilation (TTA) upconversion.

Conclusion

$\text{C}^*\text{N}^*\text{N}$ ligand with five–six fused coordination structure and the $\text{C}^*\text{N}^*\text{N}$ ligands with five–five fused coordination structure were used for preparation of six Pt(II) complexes. For each coordination profile, three different aryl acetylide ligands i.e. naphthalenedimide (NDI), pyrenyl (Py) and naphaleneimide (NI) acetylides were used for the preparation of the complexes. The aim is to study the synergic effect of both the $\text{C}^*\text{N}^*\text{N}$ or $\text{C}^*\text{N}^*\text{N}$ ligands ligand and the aryl acetylide ligands on the photoredox and photophysical properties of the complexes. The electrochemical property of the complexes were studied with cyclic voltammetry, and the photophysical properties of the complexes were studied with steady-state and time-resolved absorption and emission spectroscopies. The proper formation of $^1\text{MLCT}$ is first crucial factor for the triplet photosensitizers based on transition metal complexes, which could be fine tuned by the photoredox properties. Then, the energy level of ligand (^1IL), light harvesting antenna, at singlet excited state should be close or higher than that of $^1\text{MLCT}$, which benefit for the $^1\text{IL} \rightarrow ^1\text{MLCT} \rightarrow ^3\text{MLCT}$ process. The triplet excited states are in intraligand feature and are with long lifetime (**Pt-4**, $\tau = 90.1 \mu\text{s}$). The photophysical properties of the complexes were rationalized with DFT calculations. The complexes were used as triplet photosensitizers for triplet–triplet annihilation upconversion and upconversion quantum yields up to 29.7% were observed. These results are useful for future designing of the Pt(II) complexes which show RT phosphorescence and long-lived triplet excited states.

Acknowledgments

We thank the NSFC (21273028, 21302224, 51172285, 21473020 and 21421005), the Royal Society (UK) and NSFC (Cost-Share-21011130154), Program for Changjiang Scholars and Innovative Research Team in University [IRT_13R06], Ministry of Education (SRFDP-20120041130005), Technology Program for Basic Research of Qingdao (14-2-4-47-jch), Shandong Provincial Natural Science Foundation (ZR2013BQ028), China Postdoctoral Science Foundation (2014M560590), State Key Laboratory of Fine Chemicals (KF1203), and the Fundamental Research Funds for the Central Universities (DUT14ZD226, DUT2013TB07, 13CX02066A, 14CX02060A) for financial support.

Note

^a State Key Laboratory of Heavy Oil Processing, China University of Petroleum, Qingdao 266580, P.R. China. Fax: +86 532 8698 1787, Tel.: +86 532 8698 3452. E-mail: wumb@upc.edu.cn

^b State Key Laboratory of Fine Chemical, School of Chemical Engineering, Dalian University of Technology, Dalian, 116024, P. R. China. E-mail: zhaojzh@dlut.edu.cn; Web: <http://finechem2.dlut.edu.cn/photochem>.

† Electronic Supplementary Information (ESI) available: synthesis detail, molecular structure characterization data and more spectra. See DOI: 10.1039/b000000x/

References

- S. Chan, Y. Wang, C. Che, K. Cheung and N. Zhu. *Chem.–Eur. J.*, 2001, **7**, 4180–4190.
- X. Wang, S. Goeb, Z. Ji, N. A. Pogulaichenko and F. N. Castellano. *Inorg. Chem.*, 2011, **50**, 705–707.
- K. Lo, A. Choi and W. Law. *Dalton Trans.*, 2012, **41**, 6021–6047.
- A. Tam and V. Yam. *Chem. Soc. Rev.*, 2013, **42**, 1540–1567.
- E. Bagdaley, J. A. Weinstein and J. Williams. *Coord. Chem. Rev.*, 2012, **256**, 1762–1785.
- (a) A. Rachford, F. Hua, C. J. Adams and F. N. Castellano. *Dalton Trans.*, 2009, **20**, 3950–3954; (b) W. Wu, P. Yang, L. Ma, J. Lalevée and J. Zhao. *Eur. J. Inorg. Chem.*, 2012, **2**, 228–231.
- F. Dai, H. Zhan, Q. Liu, Y. Fu, J. Li, Q. Wang, Z. Xie, L. Wang, F. Yan and W. Wong. *Chem. Eur. J.*, 2012, **18**, 1502–1511.
- T. N. S. Rachford and F. N. Castellano, *Coord. Chem. Rev.*, 2010, **254**, – 2573.
- J. Zhao, S. Ji and H. Guo. *RSC Adv.*, 2011, **1**, 937–950.
- P. Ceroni. *Chem. Eur. J.*, 2011, **17**, 9560–9564.
- Y. Ho, C. Koo, K. Wong, H. Kong, C. Chan, W. Kwok, C. Chow, M. Lam and W. Wong. *Dalton Trans.*, 2012, **41**, 1972–1800.
- D. Ravindranathan, D. A. Vezzu, L. Bartolotti, P. D. Boyle and S. Huo. *Inorg. Chem.*, 2010, **49**, 8922–8928.
- D. A. Vezzu, D. Ravindranathan, A. W. Garner, L. Bartolotti, M. E. Smith, P. D. Boyle and S. Huo. *Inorg. Chem.*, 2011, **50**, 8261–8273.
- H. Guo, M. L. Muro-Small, S. Ji, J. Zhao and F. N. Castellano. *Inorg. Chem.*, 2010, **49**, 6802–6804.
- F. N. Castellano, I. E. Pomestchenko, E. Shikhova, F. Hua, M. L. Muro-Small and N. Rajapakse. *Coord. Chem. Rev.*, 2006, **250**, 1819–1828.
- E. O. Danilov, I. E. Pomestchenko, S. Kinayyigit, P. L. Gentili, M. Hissler, R. Ziessel and F. N. Castellano. *J. Phys. Chem. A.*, 2005, **103**, 2465–2471.
- I. E. Pomestchenko and F. N. Castellano. *J. Phys. Chem. A.*, 2004, **108**, 3485–3492.
- A. A. Rachford, S. Goeb, R. Ziessel and F. N. Castellano. *Inorg. Chem.*, 2008, **47**, 4348–4355.
- F. Hua, S. Kinayyigit, J. R. Cable and F. N. Castellano. *Inorg. Chem.*, 2005, **44**, 471–473.
- W. Wu, L. Liu, X. Cui, C. Zhang and J. Zhao. *Dalton Trans.*, 2013, **42**, 14374–14379.
- S. Ji, W. Wu, J. Zhao, H. Guo and W. Wu. *Eur. J. Inorg. Chem.*, 2012, **19**, 3183–3190.
- Y. Liu, W. Wu, J. Zhao, X. Zhang and H. Guo. *Dalton Trans.*, 2011, **40**, 9085–9089.
- L. Huang, L. Zeng, H. Guo, W. Wu, W. Wu, S. Ji and J. Zhao. *Eur. J. Inorg. Chem.*, 2011, **29**, 4527–4533.
- W. Wu, J. Zhao, W. Wu and Y. Chen. *J. Organomet. Chem.*, 2012, **713**, 189–196.
- H. Sun, H. Guo, W. Wu, X. Liu and J. Zhao. *Dalton Trans.*, 2011, **40**, 7834–7841.
- (a) D. Ravelli, D. Dondi, M. Fagnoni and A. Albinì, *Chem. Soc. Rev.*, 2009, **38**, 1999–2011; (b) M. L. Marin, L. Santos-Juanes, A. Arques, A. M. Amat and M. A. Miranda, *Chem. Rev.*, 2012, **112**, 1710–1750; (c) W. Wu, Y. Geng, W. Fan, Z. Li, L. Zhan, X. Wu, J. Zheng, J. Zhao and M. Wu. *RSC Adv.*, 2014, **4**, 51349–51352.
- C. F. Harris, D. A. Vezzu, L. Bartolotti, P. D. Boyle and S. Huo. *Inorg. Chem.*, 2013, **52**, 11711–11722.
- W. Wu, D. Huang, X. Yi and J. Zhao. *Dyes Pigments*, 2013, **96**, 220–231.
- M. J. Frisch, G. W. Trucks, H. B. Schlegel, G. E. Scuseria, M. A. Robb, J. R. Cheeseman, G. Scalmani, V. Barone, B. Mennucci, G. A. Petersson, H. Nakatsuji, M. Caricato, X. Li, H. P. Hratchian, A. F.

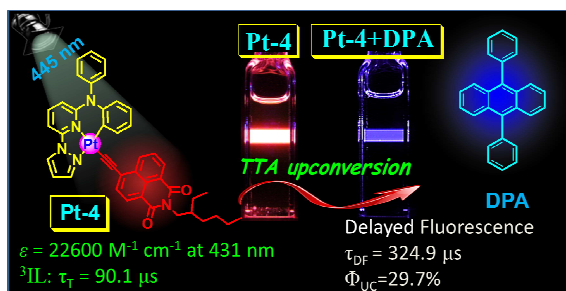
- Izmaylov, J. Bloino, G. Zheng, J. L. Sonnenberg, M. Hada, M. Ehara, K. Oyota, R. Fukuda, J. Hasegawa, M. Ishida, T. Nakajima, Y. Honda, O. Kitao, H. Nakai, T. Vreven, J. A. Montgomery Jr., J. E. Peralta, F. Ogliaro, M. Bearpark, J. J. Heyd, E. Brothers, K. N. Kudin, V. N. Staroverov, R. Kobayashi, J. Normand, K. Raghavachari, A. Rendell, J. C. Burant, S. S. Iyengar, J. Tomasi, M. Cossi, N. Rega, N. J. Millam, M. Klene, J. E. Knox, J. B. Cross, V. Bakken, C. Adamo, J. Jaramillo, R. Gomperts, R. E. Stratmann, O. Yazyev, A. J. Austin, R. Cammi, C. Pomelli, J. W. Ochterski, R. L. Martin, K. Morokuma, V. G. Zakrzewski, G. A. Voth, P. Salvador, J. J. Dannenberg, S. Dapprich, A. D. Daniels, Ö. Farkas, J. B. Foresman, J. V. Ortiz, J. Cioslowski, D. J. Fox, Gaussian 09 Revision A.1, Gaussian Inc., Wallingford CT, Cioslowski, D. J. Fox, *Gaussian 09 Revision A.1*, Gaussian Inc., Wallingford CT, 2009.
- 15 30 Q. Li, H. Guo, L. Ma, W. Wu, Y. Liu and J. Zhao. *J. Mater. Chem.*, 2012, **22**, 5319–5329.
- 31 Z. Dai, A. J. Metta-Magaña and J. E. Nuñez. *Inorg. Chem.*, 2014, **53**, 7188–7196.
- 32 T. Yogo, Y. Urano, Y. Ishisuka, F. Maniwa and T. Nagano, *J. Am. Chem. Soc.*, 2005, **127**, 12162–12163.
- 20 33 (a) X. Zhang, L. Chi, S. Ji, Y. Wu, P. Song, K. Han, H. Guo, T. D. James and J. Zhao. *J. Am. Chem. Soc.*, 2009, **131**, 17452–17463; (b) D. Rehm and A. Weller. *J. Chem.*, 1970, **8**, 259–271; (c) Z. R. Grabowski and J. Dobkowski, *Pure. Appl. Chem.*, 1983, **55**, 245–252.
- 25 34 J. Zhao, W. Wu, J. Sun and S. Guo. *Chem. Soc. Rev.*, 2013, **42**, 5323–5351.
- 35 W. Wu, J. Zhao, H. Guo, J. Sun, S. Ji and Z. Wang. *Chem. Eur. J.*, 2012, **18**, 1961–1968.
- 36 K. Hanson, A. Tamayo, V. V. Diev, M. T. Whited, P. I. Djurovich and M. E. Thompson. *Inorg. Chem.*, 2010, **49**, 6077–6084.
- 30 37 P. Yang, W. Wu, J. Zhao, D. Huang and X. Yi. *J. Mater. Chem.*, 2012, **22**, 20273–20283.
- 38 A. Monguzzi, R. Tubino, S. Hoseinkhani, M. Campione and F. Meinardi. *Phys. Chem. Chem. Phys.*, 2012, **14**, 4322–4332.
- 35 39 Y. C. Simon and C. Weder. *J. Mater. Chem.*, 2012, **22**, 20817–20830.
- 40 J. Zhao, S. Ji, W. Wu, W. Wu, H. Guo, J. Sun, H. Sun, Y. Liu, Q. Li and L. Huang, *RSC Adv.*, 2012, **2**, 1712–1728.

40

45

Graphical abstract

Synergetic effect of C^{*}N[^]N/C[^]N[^]N coordination and the arylacetylide ligands on the photophysical properties of cyclometalated platinum complexes

Wenting Wu,^{a,b} Xueyan Wu,^a Jianzhang Zhao^{b*} and Mingbo Wu^{a,*}

C^{*}N[^]N and C[^]N[^]N coordinated Pt(II) complexes with different arene acetylides ligands were prepared and the photophysical properties were studied.